

1 **E-00380-2018: Revised version**

2

3 **Calcium signaling and secretory granule pool dynamics underlie biphasic**
4 **insulin secretion and its amplification by glucose: experiments and**
5 **modeling**

6

7

8 **Morten Gram Pedersen^{1,2,3,*}, Alessia Tagliavini¹ and Jean-Claude Henquin⁴**

9

10 1. *Department of Information Engineering, University of Padova, Italy*

11 2. *Department of Mathematics "Tullio Levi-Civita", University of Padova, Italy*

12 3. *Padova Neuroscience Center, University of Padova, Italy*

13 4. *Unit of Endocrinology and Metabolism, Faculty of Medicine, University of*
14 *Louvain, Brussels, Belgium*

15

16 * Corresponding author:

17

18 Department of Information Engineering

19 University of Padova

20 Via Gradenigo 6/B

21 35131 Padova

22 Italy

23

24 email: pedersen@dei.unipd.it

25 tel: +39 049 827 7961

26 fax: +39 049 827 7699

27

28

29

30 *Author contributions:*

31 - MGP developed models, wrote computer code, performed simulations, analyzed
32 data, and wrote the manuscript.

33 - AT wrote computer code and performed simulations.

34 - JCH performed experiments, analyzed data, and wrote the manuscript.

35

36 *Running head:*

37 Ca^{2+} signals and granule pools in biphasic insulin secretion

38

39 -----

40

41

42 Abstract (244 words)

43

44 Glucose-stimulated insulin secretion from pancreatic β -cells is controlled by a
45 triggering pathway culminating in calcium influx and regulated exocytosis of
46 secretory granules, and a less understood amplifying pathway that augments
47 calcium-induced exocytosis. In response to an abrupt increase in glucose
48 concentration, insulin secretion exhibits a first peak followed by a lower
49 sustained second phase. This biphasic secretion pattern is disturbed in diabetes.
50 It has been attributed to depletion and subsequent refilling of a readily-
51 releasable pool of granules or to the phasic cytosolic calcium dynamics induced
52 by glucose. Here we apply mathematical modeling to experimental data from
53 mouse islets to investigate how calcium and granule pool dynamics interact to
54 control dynamic insulin secretion. Experimental calcium traces are used as
55 inputs in three increasingly complex models of pool dynamics, which are fitted to
56 insulin secretory patterns obtained using a set of protocols of glucose and
57 tolbutamide stimulation. New calcium and secretion data for so-called staircase
58 protocols, where the glucose concentration is progressively increased, are
59 presented. These data can be reproduced without assuming any heterogeneity in
60 the model, in contrast to previous modeling, because of nontrivial calcium
61 dynamics. We find that amplification by glucose can be explained by increased
62 mobilization and priming of granules. Overall, our results indicate that calcium
63 dynamics contribute substantially to shaping insulin secretion kinetics, which
64 implies that better insight into the events creating phasic calcium changes in
65 human β -cells is needed to understand the cellular mechanisms that disturb
66 biphasic insulin secretion in diabetes.

67

68

69 Keywords70 β -cells, pancreatic islets, calcium dynamics, exocytosis, mathematical model

71

72

73

74 Glossary

75 RRP: Readily releasable pool;

76 $[Ca^{2+}]_i$: cytosolic free calcium concentration

77 INTRODUCTION

78

79 Glucose-induced insulin secretion requires operation of two complementary
80 mechanisms in pancreatic β -cells: an increase in the cytosolic free calcium
81 concentration $[Ca^{2+}]_i$ that triggers exocytosis of insulin granules and actuation of
82 an amplifying pathway that augments the exocytotic response to calcium (25).
83 The amplifying signals derive from glucose metabolism, but their exact
84 biochemical nature is still uncertain (15, 25, 33).

85

86 It has long been known that a rapid and sustained increase in blood
87 glucose induces a biphasic rise in plasma insulin concentrations in normal
88 human subjects (5, 7). This peculiar insulin kinetics is due to the biphasic
89 dynamics of insulin secretion by pancreatic β -cells as calculated by C-peptide
90 deconvolution (62, 63) and directly established by in vitro studies using isolated
91 human islets (26, 56). Although produced only by unphysiologically rapid
92 glucose stimulations, this biphasic insulin response of β -cells has attracted
93 considerable attention because a low first phase has proved to be predictive of a
94 deterioration of glucose homeostasis (8, 45, 54). In patients with impaired
95 glucose tolerance or overt diabetes, both phases are impaired (19, 30, 52, 54)
96 with sometimes (62, 64) though not always (19, 30) a greater impact on the first
97 phase. Elucidation of the cellular mechanisms underlying biphasic insulin
98 secretion thus has clinical implications. Achieving such a goal however rests on
99 accessible experimental models.

100

101 A biphasic dynamics also characterizes glucose-induced plasma insulin
102 changes (29, 46) and in vitro insulin secretion (11, 35, 37) in rodents. To explain
103 the two phases of insulin secretion observed in the perfused rat pancreas,
104 Grodsky (21, 22) proposed a model, where a limited pool of readily releasable
105 insulin "packets" was secreted quickly to create the first phase, and subsequent
106 refilling of the pool was responsible for the second phase. He also modeled the
107 so-called staircase protocol where the glucose stimulus is increased in small
108 steps, each giving rise to a first-phase-like peak of insulin, by assuming that the
109 readily releasable insulin pool is heterogeneous, containing insulin packets with
110 different glucose-thresholds (21). According to an alternative model, proposed
111 by Cerasi et al. (6), the two phases of insulin secretion result from the interaction
112 of inhibitory and potentiating signals with different kinetics. Subsequent studies
113 (36, 47) compared the storage- and signal-limited models, found that both have
114 caveats, and concluded that a combined model with both limited insulin pools
115 and time-dependent signals performed better. However, the cellular origin of the
116 heterogeneity of the releasable pool of insulin and the biochemical nature of the
117 putative inhibitory and potentiating signals remained elusive.

118

119 Studies of exocytosis in single β -cells provided substantial support to the
120 pool model, with depletion of a readily releasable pool (RRP) yielding the first
121 phase, while refilling of the RRP creating the second phase (2, 10, 48, 58). It was
122 further suggested that cell-to-cell heterogeneity seen in $[Ca^{2+}]_i$ imaging
123 experiments (32) could underlie the postulated threshold distribution for the
124 RRP (50). Although β -cell coupling through gap-junctions within islets reduces
125 intercellular heterogeneity substantially (59, 60) and synchronizes cellular

126 responses (49, 55), recent evidence indicates that some heterogeneity persists
127 between β -cells and islets (3, 39), possibly accounting for RRP heterogeneity.

128

129 The most obvious signal capable of inducing biphasic insulin secretion is
130 the triggering $[\text{Ca}^{2+}]_i$, the increase of which follows a biphasic kinetic in glucose
131 stimulated β -cells (13, 25, 28). Such a view is supported by experiments showing
132 that all maneuvers interfering with the rapid rise in $[\text{Ca}^{2+}]_i$ alter the first phase
133 and that all agents inducing a rapid $[\text{Ca}^{2+}]_i$ rise induce a rapid secretion (25, 28).
134 However, against this interpretation speak observations of biphasic insulin
135 secretion in face of virtually sustained elevations of $[\text{Ca}^{2+}]_i$ produced by
136 tolbutamide or KCl (28, 43). Whether amplifying signals and or depletion of a
137 limited amount of releasable insulin contribute to the phasic insulin pattern
138 under these conditions is unclear.

139

140 In the present study we combined experimental measurements of $[\text{Ca}^{2+}]_i$
141 and insulin secretion in mouse islets with mathematical modeling to unravel the
142 contributions of $[\text{Ca}^{2+}]_i$ signals and pool dynamics to biphasic insulin secretion.
143 Our analysis shows that triggering signals and granular pools both contribute to
144 shape the biphasic release pattern, and uncovers mechanisms underlying
145 amplification by glucose of the secretory response to calcium.

146

147

148

149 **MATERIALS AND METHODS**

150

151 *Experiments*

152

153 All experiments were performed with islets isolated from the pancreas of female
154 C57BL6 mice. After hand selection, the islets were cultured overnight in RPMI
155 medium containing 10 mM glucose, and then used for dynamic measurements of
156 insulin secretion or $[\text{Ca}^{2+}]_i$. All methods were exactly as described in our
157 previous studies (29, 43). Because all presented traces correspond to averages
158 of results obtained with several islets, oscillations in $[\text{Ca}^{2+}]_i$ and insulin secretion
159 present in individual islets are masked, whereas the biphasic dynamics of these
160 responses are preserved.

161

162 *Mathematical modeling*

163

164 Our aim was to study the impact of $[\text{Ca}^{2+}]_i$ dynamics on insulin secretion. We
165 developed various models of granule pool dynamics that were driven by the
166 experimentally recorded $[\text{Ca}^{2+}]_i$ traces (see Fig. 1). Simulated secretion profiles
167 were then fitted to experimental insulin patterns to investigate which models
168 were able to fit the data satisfactorily. The models were described by ordinary
169 differential equations, where some of the transition rates between different
170 pools depended on the glucose concentration, whereas the combined
171 exocytosis/secretion rate depended on the time-varying experimentally
172 recorded $[\text{Ca}^{2+}]_i$ traces. Parameter estimation was not our scope, and
173 identifiability issues and estimation accuracy were neglected.

174

175 Model 1

176 In this model, only a readily-releasable pool (*RRP*) is present. This pool is refilled
 177 by a “mobilization” or “refilling” process with rate $M(G)$ depending on the
 178 glucose concentration G from an infinite reserve pool. The RRP granules can
 179 undergo fusion and secretion with rate $S(Ca)$ depending linearly on $[Ca^{2+}]_i$ above
 180 a threshold (31, 49). Granules can also undergo glucose-independent
 181 “internalization” or “loss-of-release-capability” with rate N from the RRP. The
 182 instantaneous secretion is thus $RRP(t) * S(Ca(t))$. We assume that insulin I to be
 183 fitted to the experimental data is measured from a reservoir described by first-
 184 order kinetics with a time-constant of 1 min, i.e.,

$$185 \quad dI/dt = (S * RRP - I) / (1 \text{ min}).$$

186 This model has 10 parameters to be estimated.

187

188 Model 2

189 This model adds an intermediate pool X located near or at the plasma membrane
 190 to model 1. The granule pool X is refilled from an infinite reserve pool with rate
 191 $M(G)$ depending on the glucose concentration G . From the pool X , the granules
 192 enter the RRP following glucose-dependent priming with rate $p(G)$. As in model
 193 1, the RRP granules may be released with rate $S(Ca)$. Granules can also undergo
 194 glucose-independent “unpriming” with rate q from the RRP, and glucose-
 195 independent internalization with rate N from X . Model 2 has 18 parameters to be
 196 estimated.

197

198 Model 3

199 In this model, glucose-independent mobilization directly to, and internalization
 200 from, the RRP with rate k , respectively l , was added to Model 2. Such direct
 201 mobilization bypassing the pool X may represent “basal” mobilization and is
 202 accessible to tolbutamide- or potassium-induced $[Ca^{2+}]_i$ elevations. Model 3 has
 203 20 parameters to be estimated.

204

205

206 **Data fitting**

207

208 For each model, we fixed the parameters and simulated 14 different protocols
 209 corresponding to the experimental data. The parameters M and p were allowed
 210 to change with glucose levels (assuming the same value for 10 mM and 11.1 mM
 211 glucose to reduce the number of parameters to fit). For experiments with pre-
 212 stimulation in 3 mM glucose (rows 1, 3 and 4 in Fig. 2), the initial conditions for
 213 the pool sizes were set so that the model was in steady-state in the absence of
 214 secretion. For experiments with pre-stimulation in 8.5 mM glucose (row 2 in Fig.
 215 2), the initial conditions were set to the final value of the model simulation after
 216 a step from 3 mM to 8.5 mM glucose.

217

218 The parameters were then varied automatically within the optimization
 219 algorithm, and the simulated secretion data were compared to the experimental
 220 recordings to minimize the squared error, calculated as the difference between
 221 simulated (I) and experimental insulin data for the 14 protocols. In order to
 222 exploit the information from the relatively few tolbutamide protocols, we

223 weighted the residuals from fitting of the experiments from Mourad et al. (43) 10
224 times higher.

225

226 The procedure was repeated with different initial choices of the
227 parameter set, to reduce the risk of ending in a local minimum, and eventually
228 led to a single parameter vector for which the model fit to the 14 experimental
229 data sets was optimal. Model parameters were constrained so that mobilization
230 and priming were non-decreasing functions of glucose. In other fits no
231 constraints were imposed, allowing mobilization and priming rates to be non-
232 monotone functions of glucose, hence permitting extra degrees of freedom for
233 the estimation of parameters.

234

235 Simulations were done in MATLAB (version R2017b; Mathworks Inc.)
236 using the ode45 solver. Fitting was performed with the fmincon function. The
237 computer code is available at <http://www.dei.unipd.it/~pedersen>

238

239

240 **RESULTS**

241

242 *Experimental data description*

243

244 We fitted our mathematical models to reproduce results from previously
245 published (29, 43) and novel studies of phasic islet $[Ca^{2+}]_i$ changes and insulin
246 secretion in response to different protocols of glucose or tolbutamide
247 stimulation (Fig. 2).

248

249 In a first series of experiments, taken from (29), brisk jumps of glucose
250 from 3 mM to 8.5, 11.1, 16.7 or 30 mM in perfusion medium resulted in biphasic
251 insulin secretion and $[Ca^{2+}]_i$ elevation (Fig. 2, A-D). The first phases of secretion
252 and $[Ca^{2+}]_i$ increased in both amplitude and duration with increasing glucose
253 concentration. Second phases of secretion and $[Ca^{2+}]_i$ also increased with
254 glucose. In a second series, islets were initially exposed to 8.5 mM glucose before
255 being stimulated with 11.1, 16.7 or 30 mM glucose (Fig. 2, E-G). Both insulin and
256 $[Ca^{2+}]_i$ responses were again biphasic, but first phases were smaller than after
257 initial perfusion in 3 mM glucose, whereas second phases were similar.

258

259 A third series of experiments, taken from (43), compared insulin and
260 $[Ca^{2+}]_i$ responses in islets subjected to stimulation with 15 mM glucose or 500
261 μ M tolbutamide in 3 mM glucose (Fig. 2, H-K). Salient differences and similarities
262 were identified. Sustained stimulation with either stimulus induced a clearly
263 biphasic secretion of insulin although the dynamics of the $[Ca^{2+}]_i$ response
264 evoked by tolbutamide was hardly biphasic compared to that evoked by glucose
265 (Fig. 2, H vs. I). Tolbutamide-induced secretion was about 50% smaller than
266 glucose-induced secretion in the face of a slightly greater elevation of $[Ca^{2+}]_i$, a
267 difference that reflects amplification of insulin secretion by glucose. Application
268 of short pulses of tolbutamide or glucose, to mimic several first phases, again
269 induced roughly similar $[Ca^{2+}]_i$ responses but smaller insulin responses with
270 tolbutamide than glucose (Fig. 2, J vs. K). With each stimulus, the amplitude of
271 the first insulin pulse was slightly larger than that of subsequent pulses.

272
273
274 Finally, in a series of novel experiments, islets were stimulated using
275 staircase increases in glucose concentration from 3 to 7, 10 and eventually 15
276 mM (Fig. 2, L-N). When steps at 7 and 10 mM glucose were short (5 min), a
277 distinct $[Ca^{2+}]_i$ peak was produced by every increase in glucose concentration,
278 which was accompanied by a peak of insulin secretion (Fig. 2L). Applying longer
279 glucose steps (20 min) did not substantially change the pattern (Fig. 2M); a small
280 second phase evolved at 7 and 10 mM glucose, but the peaks evoked by each
281 increase in glucose had a similar size to the ones evoked by short steps. Notably,
282 the first phase of the $[Ca^{2+}]_i$ response to 15 mM glucose was much longer, though
283 not greater in amplitude, following the single step directly from 3 mM glucose
284 than during the staircase protocol (step from 10 mM glucose) and the
285 corresponding first phase of insulin secretion was considerably larger (Fig. 2N).
286 Second phases were similar. Omission of extracellular calcium, while keeping
287 glucose at 15 mM, markedly lowered islet $[Ca^{2+}]_i$ and stopped insulin secretion.
288 Reintroduction of calcium elicited rapid increases in $[Ca^{2+}]_i$ and secretion, but
289 the insulin peak was smaller than that observed after a step from 3 to 15 mM
290 glucose although the $[Ca^{2+}]_i$ response was not smaller (Fig. 2N).

291
292 We next used these 14 experimentally recorded $[Ca^{2+}]_i$ traces as inputs to
293 models of insulin release. The simulated secretion profiles were then fitted to
294 the corresponding experimental insulin patterns. As explained above, three
295 models of increasing complexity were compared.

296 297 298 ***Performance of Model 1***

299
300 The simple Model 1, with a single pool, fitted the data acceptably but
301 underestimated the peaks when glucose was stepped from 3 mM to 8.5, 11.1,
302 16.7 or 30 mM (Fig. 3, A-D, red curves), and overestimated the peak after
303 reintroduction of calcium in 15 mM glucose (Fig. 3, L and N). This latter
304 discrepancy could be corrected (not shown), in this and in Models 2 and 3 to be
305 discussed below, by assuming lower refilling rate at low $[Ca^{2+}]_i$ levels (23).
306 During stimulation with 8.5 mM glucose, the RRP was nearly constant (Fig. 4A).
307 The smaller size of the peaks observed when stepping to 16.7 or 30 mM glucose
308 occurred from 8.5 mM (Fig. 3F and G) rather than 3 mM glucose (Fig. 3C and D)
309 was almost entirely due to the shorter duration of the first-phase $[Ca^{2+}]_i$ signals
310 following pre-exposure to 8.5 mM glucose (Fig. 2).

311
312 As shown in Fig. 2 (panels H-K), tolbutamide in 3 mM glucose evoked
313 slightly larger increases in $[Ca^{2+}]_i$ than did 15 mM glucose, but the resulting
314 secretion of insulin was larger with glucose than tolbutamide; that difference
315 was observed during the two phases of a sustained stimulation and during
316 application of repetitive pulses. Model 1 reproduced these differences
317 reasonably, though the first peak of tolbutamide-stimulated secretion was
318 slightly overestimated (Fig. 3H and J), and the first phase of secretion triggered
319 by 15 mM glucose slightly underestimated (Fig. 3I and K) in the model.

320

321 Model 1 was also able to reproduce the staircase experiments (Fig. 3L and
322 M). In response to each step in glucose, simulated insulin secretion showed a
323 peak, which was driven by $[Ca^{2+}]_i$ dynamics, not pool depletion, since the RRP
324 was nearly constant during the staircase protocols (Fig. 4F). This contrasts with
325 Grodsky's model (21), which postulated heterogeneity of the RRP, the peak of
326 secretion induced by each glucose step being attributed to release of subpools of
327 granules with increasing glucose-thresholds. In our model these insulin peaks
328 were purely due to the peaks in the $[Ca^{2+}]_i$ signal (Fig. 2L and M).

329

330 The estimated refilling rate remained at the basal value up to ~ 10 mM
331 glucose, after which it increased, yielding an overall sigmoidal dependence on
332 glucose concentration (Fig. 3O, red curve). When the constraint that refilling as a
333 function of glucose be non-decreasing throughout was removed, no noticeable
334 improvement in the model fits was observed, and the overall results were as
335 described above (Fig. 3, blue curves).

336

337 Thus, within the physiological range of glucose concentrations, Model 1
338 predicted that differences in secretion measured in the various protocols were
339 largely due to the different $[Ca^{2+}]_i$ signals. Pool depletion played a role at higher
340 glucose levels and during tolbutamide stimulation (Fig. 4B, D and E).

341

342 In the model, tolbutamide acted (via Ca^{2+}) only on secretion $S(Ca)$ and the
343 relatively low peak of secretion in response to tolbutamide (Fig. 2H and J)
344 imposed a limit on the estimate of the initial size of RRP. A limited pool in turn
345 resulted in a low simulated peak when glucose was stepped to 8.5 mM (Fig. 3A),
346 since the refilling rate M could not be too large in order for the model to
347 reproduce the nearly absent second phase of secretion at 8.5 mM. The same
348 problem was seen at the other levels of glucose. In other words, in this simple
349 Model 1 there was a contradiction between the low peak of secretion seen in
350 response to tolbutamide and the relatively large first phase of secretion in
351 response to glucose. We therefore analyzed the results with a slightly more
352 complicated model.

353

354

355 ***Performance of Model 2***

356

357 Compared to Model 1, Model 2 has an additional intermediate pool X between
358 mobilization and the RRP (see Fig. 1), which could correspond to docked but
359 unprimed granules (9, 13, 16, 65). This model simulated most data sets well,
360 except for the insulin peaks following glucose steps from 3 mM to 8.5 or 11.1
361 mM, which were much larger in the experiments compared to the simulated data
362 (Fig. 5A and B, red curves). This discrepancy was caused by the restrictions on
363 the priming and mobilization rates, which were imposed to be non-decreasing
364 functions of glucose. Indeed, when this constraint was removed, Model 2 was
365 able to fit the data much better, which resulted in a U-shaped glucose-
366 dependence of the mobilization rate (Fig. 5, blue curves).

367

368

369 When priming and mobilization rates were constrained to be non-
decreasing functions of the glucose concentration, the priming and refilling rates

370 were estimated to be low (Fig. 5O). This assured that 8.5 mM glucose did not
371 increase the RRP (Fig. 6A) to avoid that a subsequent rise in the $[Ca^{2+}]_i$ signal led
372 to a too large insulin peak when glucose was raised further (Fig. 5, E-G). Since the
373 priming rate at 8.5 mM is small (Fig. 5O), precluding recruitment from the
374 intermediate pool X (Fig. 6A, thin line), the simulated first phase at 8.5 mM
375 glucose was small compared to the experiments (Fig. 5A).
376

377 The simulated first peak of insulin was larger upon stepping from 3 to
378 11.1 rather than 8.5 mM glucose (Fig. 5, B vs. A) because the priming rate was
379 increased. However, to fit the still low rate of second-phase secretion measured
380 in 11.1 mM glucose, the increase in mobilization and priming rates had to be
381 limited in the model (Fig. 5O). This explains why the simulated first peak
382 remained lower than the experimental first phase (Fig. 5B). At higher glucose
383 concentrations the fits were excellent, except for a minor discrepancy when
384 stepping from 8.5 mM to 30 mM glucose (Fig. 5G), where the experimental
385 trough following the first phase was absent in the model fit. This discrepancy is
386 related to the rising second phase of secretion in the data, which the model is
387 unable to capture. Similarly to Model 1, the RRP and the pool X were nearly
388 constant during 8.5 mM glucose stimulation (Fig. 6A). The smaller secretory
389 responses to 16.7 or 30 mM glucose observed after pre-exposure to 8.5 rather
390 than 3 mM glucose (Fig. 5F and G vs C and D) were mainly due to differences in
391 the Ca^{2+} responses.
392

393 Fits to experimental data obtained during constant or intermittent
394 stimulations with tolbutamide or 15 mM glucose were excellent (Fig. 5, H-K). In
395 particular, the second, third and fourth pulses were reduced compared to the
396 first ones (Fig. 5J and K) because the intermediate pool X and the RRP only
397 refilled partly between stimuli (Fig. 6, D and E). Also, the staircase experiments
398 were reproduced very well (Fig. 5L and M).
399

400 According to Model 2, estimated priming and mobilization rates were
401 glucose-independent up to ~ 10 mM (Fig. 5O), suggesting that changes in the
402 $[Ca^{2+}]_i$ profiles were entirely responsible for the differences in secretion within
403 this physiologically relevant range.
404

405

406 ***Performance of Model 3***

407

408 Model 3 has an additional glucose-independent path refilling the RRP. The model
409 fitted the data very well, even when priming and mobilization rates were
410 constrained to increase with glucose (Fig. 7, red curves). No significant
411 improvement was obtained when this assumption was relaxed (Fig. 7, blue
412 curves). This model was able to reproduce the substantial peaks of secretion
413 when stepping from 3 mM to 8.5 or 11.1 mM glucose and above (Fig. 7, A-D).
414 Stimulation with 8.5 mM glucose depleted the intermediate pool X almost
415 completely (Fig. 8A), because priming was stimulated but refilling was not at this
416 glucose level. Subsequent steps in glucose therefore led to smaller first-phase
417 peaks, since first-phase secretion was mostly due to glucose-dependent
418 recruitment of X. Thus, in contrast to the two previous models, Model 3

419 attributed to pool depletion (of X) a major role in explaining the differences
420 following 3 mM or 8.5 mM pre-exposure.

421

422 As for Model 2, tolbutamide and staircase experiments were reproduced
423 well, although Model 3 slightly overestimated the first peaks in response to the
424 steps to 7 mM and 10 mM glucose (Fig. 7L and M).

425

426 Compared to Model 2, the estimated priming rate increased with glucose
427 already below 10 mM (Fig. 7O), suggesting that both granule and $[Ca^{2+}]_i$
428 dynamics played a role in shaping release patterns under physiological
429 conditions. Indeed, depletion of X because of rapid priming (Fig. 8A) allowed the
430 model to reproduce the peak of secretion already at 8.5 mM (Fig. 7A). These
431 estimates for the glucose-dependence of the priming rate in Model 3 correspond
432 to experimental findings that amplification operates already at low glucose
433 concentrations that do not increase $[Ca^{2+}]_i$ and, therefore, do not trigger insulin
434 release on their own (25).

435

436 In contrast to Model 2, the pool size of X was nearly constant during
437 tolbutamide simulations (Fig. 8D) since the additional direct refilling route
438 allowed the model to refill the RRP between tolbutamide pulses with a very low
439 priming rate p at 3 mM glucose. This in turn permitted a very low depriming rate
440 q , which was estimated to be ~ 10 fold lower in Model 3 compared to Model 2.
441 With lower q and basal p , Model 3 was able to create large simulated peaks when
442 glucose was raised, by rapid glucose-dependent recruitment of the intermediate
443 pool X (Fig. 8A, B and E). In other words, tolbutamide acted only on the RRP,
444 whereas glucose acted on both X and RRP by recruiting X rapidly into the RRP,
445 thereby causing the two pools to behave as if they were one. Amplification by
446 higher concentrations of glucose was caused by increased mobilization of
447 granules into X followed by very rapid priming into the RRP.

448

449

450 DISCUSSION

451

452 Since it is notoriously more difficult to obtain long $[Ca^{2+}]_i$ recordings from human
453 than mouse islets, and hence to study how calcium influences insulin secretion
454 patterns through interactions with granule dynamics, we applied our modeling
455 approach to previously published and novel data from mouse islets. Our analysis
456 shows that both $[Ca^{2+}]_i$ changes and insulin granule pools contribute to biphasic
457 secretion. Our findings give biological identity to the phenomenological signals
458 proposed by Cerasi et al. (6) in the form of intracellular Ca^{2+} , while the pool
459 description is virtually as suggested from experiments (2, 48).

460

461 The mathematical models presented here give a coherent framework for
462 the integration of $[Ca^{2+}]_i$ and granule pools, and are in some sense an updated
463 version of an earlier signal-pools-model (36). Notably, we did not assume any
464 heterogeneity of the RRP, in contrast to some earlier pool models reproducing
465 the staircase protocol (21, 50). Although our pool models are rather simple
466 compared to previous, detailed but less data-driven, models of granule pool
467 dynamics (4, 9, 51), they have the advantage on being driven by measured $[Ca^{2+}]_i$

468 profiles. Pedersen and Sherman (51) also included phasic and oscillatory "[Ca²⁺]_i
469 profiles" consisting of square pulses, but with no attention to the glucose
470 dependency. Grespan et al. (20) similarly modeled calcium phenomenologically
471 in combination with the description of a single granule pool.
472

473 Using Model 2 and Model 3, which fitted the data best, we can investigate
474 the mechanisms creating the first phase of insulin release. Upon stimulation with
475 moderately elevated glucose concentrations (<10 mM), the initial [Ca²⁺]_i peak is
476 short and, in both models, a decline of the triggering signal terminates the first
477 phase of secretion, although the RRP is still not completely depleted (Figs. 6A
478 and 8A). A relevant difference between the two models is that, at moderate
479 glucose levels, the intermediate pool *X* is left nearly untouched in Model 2 (Fig.
480 6A) whereas it is rapidly recruited into the RRP in Model 3 (Fig. 8A), which
481 consequently allows this model to create a larger insulin peak than Model 2 in
482 response to moderate glucose concentrations.
483

484 At higher glucose concentrations, a longer first phase of [Ca²⁺]_i
485 contributes to increase the first phase of secretion. However, secretion rates
486 start to decline sooner than [Ca²⁺]_i (Fig. 2) (29), which might reflect progressive
487 depletion of the RRP. In both models, the intermediate pool *X* is rapidly depleted
488 by steps to glucose concentrations above 10 mM (Figs. 6B and 8B), which
489 temporarily increases the size of the RRP, and consequently augments the peaks
490 of secretion. The secretion peak is then terminated by partial depletion of the
491 RRP (Figs. 6B and 8B). In addition, granule "mobilization" towards pool *X*
492 augments with glucose above 10 mM (Figs. 50 and 70), which mainly permits
493 setting of the second phase. Since [Ca²⁺]_i also increases with glucose both
494 mechanisms contribute to augment the second phase of secretion at higher
495 glucose. Thus, both the [Ca²⁺]_i signal and refilling of the pool of releasable
496 granules, which the signal acts on, are enhanced by glucose. In contrast,
497 tolbutamide does not increase the size of the RRP but acts only via calcium.
498

499 The mechanisms generating phasic [Ca²⁺]_i changes in response to a
500 glucose step are incompletely understood. Electrical activity is also biphasic
501 under these conditions, (24, 40, 42) and underlies the biphasic rise in [Ca²⁺]_i.
502 Based on the prominent role of [Ca²⁺]_i in driving the release patterns under the
503 protocols investigated here, we encourage further studies on the mechanisms
504 involved in shaping first-phase electrical and [Ca²⁺]_i responses in healthy and
505 diabetic human β-cells.
506

507 Notably, we are able to simulate the stair-case protocol without assuming
508 any heterogeneity of the RRP. Each step of glucose is known to elicit a rapid
509 increase in electrical activity (41) that causes a new [Ca²⁺]_i peak above the
510 already elevated [Ca²⁺]_i (32). In response to the step to 7mM glucose, the [Ca²⁺]_i
511 peak is too short for complete depletion of granule pools (Figs. 4F, 6F, 8F), and
512 the trough following the first phase of secretion is due to fading of the triggering
513 [Ca²⁺]_i signal, not to pool depletion. Hence, the RRP is still nearly filled when the
514 next glucose step creates a new [Ca²⁺]_i peak, which – therefore – can produce
515 another peak of insulin secretion. This interpretation does not exclude that cell-
516 to-cell heterogeneity (3) – in particular with respect to [Ca²⁺]_i amplitude,

517 amplifying signals, or the time to cell activation (32, 61) – contributes to this
518 pattern (21, 50), but highlights that the secretion profile of the staircase protocol
519 can be largely explained by $[Ca^{2+}]_i$ dynamics. Further modeling studies should
520 aim to investigate how cell-to-cell heterogeneity in combination with dynamic
521 $[Ca^{2+}]_i$ patterns shape insulin secretion from a population of β -cells.

522
523 Glucose-dependent amplification of calcium-induced exocytosis is
524 thought to account for 50% of insulin secretion during the two phases of insulin
525 secretion in mouse (25, 43) and human islets (27). We suggest that amplification
526 of first-phase insulin secretion is caused by glucose-dependent priming of
527 granules located at or very close to the plasma membrane, likely by recruitment
528 of exocytotic proteins to the insulin granules (1, 16, 18, 65). Second-phase
529 amplification is attributed mostly to glucose-dependent “mobilization” in
530 addition to rapid priming (17). It should however be kept in mind that
531 amplification does not require a functional cytoskeleton and that “mobilization”
532 does not imply long-distance transfer of granules (43, 44). The nature of the
533 amplifying signals generated by glucose metabolism is still a matter of debate,
534 but there is evidence for rapid ATP-dependent priming in single-cell recordings
535 (14), and several other products have been suggested to be involved the second-
536 phase amplification (15, 33).

537
538 Detailed studies of the dynamics of insulin secretion by islets from Type 2
539 diabetic subjects have yet to be performed. However, perfusions of normal
540 human islets have shown that increases in the pre-stimulatory glucose
541 concentration from 3 to 6, 8 or 10 mM progressively decrease the magnitude of
542 the first phase of insulin secretion induced by 15 mM glucose (26) but augment
543 the response to tolbutamide (27). A decrease in first phase was also observed in
544 mouse islets when stepping from 8 rather than 3 mM glucose to 16 mM (Fig 2C
545 vs. F). Our models indicate that both a smaller Ca^{2+} signal and – for Model 3 –
546 reduced refilling of the RRP account for the phenomenon. We, therefore, only
547 partly agree with a recent suggestion that defects in pool refilling explain the loss
548 of first phase and the decrease of second phase insulin secretion in Type 2
549 diabetic subjects, with no need to assume disturbed $[Ca^{2+}]_i$ handling (20). There
550 is evidence that insulin granule docking and priming are disturbed in diabetic β -
551 cells (17, 18). However, arginine (38, 53) and tolbutamide (34) remain able to
552 induce a peak of insulin secretion in diabetic patients, and in islets from diabetic
553 donors in vitro (12), an effect mimicked by KCl-induced depolarization in single
554 diabetic β -cells (10, 17). These results indicate that the RRP is not empty in
555 diabetic β -cells. We, therefore, believe it unlikely that the loss of biphasic insulin
556 secretion in diabetic subjects is the result of disturbed granule dynamics only. In
557 contrast to tolbutamide, glucose is poorly able to induce electrical activity in
558 diabetic compared to healthy β -cells (57), which most likely causes disturbed
559 $[Ca^{2+}]_i$ dynamics and blunted insulin secretion (28, 57).

560
561 In summary, we propose that phasic $[Ca^{2+}]_i$ patterns contribute
562 substantially to the creation of biphasic insulin secretion patterns, in addition to
563 granule dynamics. Hence, to understand the cellular mechanisms that lead to
564 disturbed biphasic insulin release in type 2 diabetes, better insight into the

565 generation of phasic electrical activity and $[Ca^{2+}]_i$ dynamics in human β -cells is
 566 needed.

567

568

569 Grants

570 MGP was supported by the University of Padova (SID project 2017).

571

572

573 Disclosures

574 The authors have no potential conflict of interest.

575

576

577 Acknowledgments

578 The contribution of Myriam Nenquin to the experimental aspects of the study is
 579 greatly appreciated.

580

581

582

583

584 **REFERENCES**

585

586 **1. Alenkvist I, Gandasi NR, Barg S, Tengholm A.** Recruitment of Epac2A to
 587 insulin granule docking sites regulates priming for exocytosis. *Diabetes*
 588 66: 2610-2622, 2017.

589

590 **2. Barg S, Eliasson L, Renström E, Rorsman P.** A subset of 50 secretory
 591 granules in close contact with L-type Ca^{2+} channels accounts for first-phase
 592 insulin secretion in mouse beta-cells. *Diabetes* 51 Suppl 1: S74-S82, 2002.

593

594 **3. Benninger RKP, Hodson DJ.** New understanding of β -cell heterogeneity and
 595 in situ islet function. *Diabetes* 67: 537-547, 2018.

596

597 **4. Bertuzzi A, Salinari S, Mingrone G.** Insulin granule trafficking in β -cells:
 598 mathematical model of glucose-induced insulin secretion. *Am J Physiol*
 599 *Endocrinol Metab* 293: E396-E409, 2007.

600

601 **5. Blackard WG, Nelson NC.** Portal and peripheral vein immunoreactive insulin
 602 concentrations before and after glucose infusion. *Diabetes* 19: 302-306, 1970.

603

604 **6. Cerasi E, Fick G, Rudemo M.** A mathematical model for the glucose induced
 605 insulin release in man. *Eur J Clin Invest* 4: 267-278, 1974.

606

607 **7. Cerasi E, Luft R.** The plasma insulin response to glucose infusion in healthy
 608 subjects and in diabetes mellitus. *Acta Endocrinol (Copenh)* 55: 278-304, 1967.

609

610 **8. Cerasi E, Luft R, Efendic S.** Decreased sensitivity of the pancreatic beta cells
 611 to glucose in prediabetic and diabetic subjects. A glucose dose-response study.
 612 *Diabetes* 21: 224-234, 1972.

613

- 614 9. **Chen YD, Wang S, Sherman A.** Identifying the targets of the amplifying
615 pathway for insulin secretion in pancreatic beta-cells by kinetic modeling of
616 granule exocytosis. *Biophys J* 95: 2226-2241, 2008.
617
- 618 10. **Cortese G, Gandasi NR, Barg S, Pedersen MG.** Statistical frailty modeling
619 for quantitative analysis of exocytotic events recorded by live cell imaging: rapid
620 release of insulin-containing granules is impaired in human diabetic β -cells. *PLoS*
621 *One* 11: e0167282, 2016.
622
- 623 11. **Curry DL, Bennett LL, Grodsky GM.** Dynamics of insulin secretion by the
624 perfused rat pancreas. *Endocrinology* 83: 572-584, 1968.
625
- 626 12. **Del Guerra S, Lupi R, Marselli L, Masini M, Bugliani M, Sbrana S, Torri S,**
627 **Pollera M, Boggi U, Mosca F, Del Prato S, Marchetti P.** Functional and
628 molecular defects of pancreatic islets in human type 2 diabetes. *Diabetes* 54: 727-
629 735, 2005.
630
- 631 13. **Eliasson L, Abdulkader F, Braun M, Galvanovskis J, Hoppa MB, Rorsman**
632 **P.** Novel aspects of the molecular mechanisms controlling insulin secretion. *J*
633 *Physiol* 586: 3313-3324, 2008.
634
- 635 14. **Eliasson L, Renström E, Ding WG, Proks P, Rorsman P.** Rapid ATP-
636 dependent priming of secretory granules precedes Ca^{2+} -induced exocytosis in
637 mouse pancreatic B-cells. *J Physiol* 503: 399-412, 1997.
638
- 639 15. **Ferdaoussi M, MacDonald PE.** Toward connecting metabolism to the
640 exocytotic site. *Trends Cell Biol* 27: 163-171, 2017.
641
- 642 16. **Gandasi NR, Barg S.** Contact-induced clustering of syntaxin and munc18
643 docks secretory granules at the exocytosis site. *Nat Commun* 5:3914, 2014.
644
- 645 17. **Gandasi NR, Yin P, Omar-Hmeadi M, Ottosson Laakso E, Vikman P, Barg**
646 **S.** Glucose-dependent granule docking limits insulin secretion and is decreased
647 in human Type 2 diabetes. *Cell Metab* 27: 470-478, 2018.
648
- 649 18. **Gandasi NR, Yin P, Riz M, Chibalina MV, Cortese G, Lund PE, Matveev V,**
650 **Rorsman P, Sherman A, Pedersen MG, Barg S.** Ca^{2+} channel clustering with
651 insulin-containing granules is disturbed in type 2 diabetes. *J Clin Invest* 127:
652 2353-2364, 2017.
653
- 654 19. **Gerich JE.** Is reduced first-phase insulin release the earliest detectable
655 abnormality in individuals destined to develop Type 2 diabetes? *Diabetes* 51
656 Suppl 1: S117-S121, 2002.
657
- 658 20. **Grespan E, Giorgino T, Arslanian S, Natali A, Ferrannini E, Mari A.**
659 Defective amplifying pathway of β -cell secretory response to glucose in Type 2
660 diabetes: integrated modeling of in vitro and in vivo evidence. *Diabetes* 67: 496-
661 506, 2018.
662

- 663 21. **Grotsky GM**. A threshold distribution hypothesis for packet storage of
664 insulin and its mathematical modeling. *J Clin Invest* 51: 2047-2059, 1972.
665
- 666 22. **Grotsky GM, Curry D, Landahl H, Bennett L**. Further studies on the
667 dynamic aspects of insulin release in vitro with evidence for a two
668 compartmental storage system. *Acta Diabetol Lat* 6 Suppl 1: 554-578, 1969.
669
- 670 23. **Gromada J, Høy M, Renström E, Bokvist K, Eliasson L, Göpel S, Rorsman**
671 **P**. CaM kinase II-dependent mobilization of secretory granules underlies
672 acetylcholine-induced stimulation of exocytosis in mouse pancreatic B-cells. *J*
673 *Physiol* 518: 745-759, 1999.
674
- 675 24. **Henquin JC**. Regulation of insulin release by ionic and electrical events in B
676 cells. *Horm Res* 27: 168-178, 1987.
677
- 678 25. **Henquin JC**. Regulation of insulin secretion: a matter of phase control and
679 amplitude modulation. *Diabetologia* 52: 739-751, 2009.
680
- 681 26. **Henquin JC, Dufrane D, Kerr-Conte J, Nenquin M**. Dynamics of glucose-
682 induced insulin secretion in normal human islets. *Am J Physiol Endocrinol Metab*
683 309: E640-E650, 2015.
684
- 685 27. **Henquin JC, Dufrane D, Gmyr V, Kerr-Conte J, Nenquin M**.
686 Pharmacological approach to understanding the control of insulin secretion in
687 human islets. *Diabetes Obes Metab* 19: 1061-1070, 2017.
688
- 689 28. **Henquin JC, Ishiyama N, Nenquin M, Ravier MA, Jonas JC**. Signals and
690 pools underlying biphasic insulin secretion. *Diabetes* 51 Suppl 1: S60-S67, 2002.
691
- 692 29. **Henquin JC, Nenquin M, Stiernet P, Ahren B**. In vivo and in vitro glucose-
693 induced biphasic insulin secretion in the mouse: pattern and role of cytoplasmic
694 Ca²⁺ and amplification signals in β -cells. *Diabetes* 55: 441-451, 2006.
695
- 696 30. **Hosker JP, Rudenski AS, Burnett MA, Matthews DR, Turner RC**. Similar
697 reduction of first- and second-phase B-cell responses at three different glucose
698 levels in type II diabetes and the effect of gliclazide therapy. *Metabolism* 38:767-
699 772, 1989.
700
- 701 31. **Jonas JC, Gilon P, Henquin JC**. Temporal and quantitative correlations
702 between insulin secretion and stably elevated or oscillatory cytoplasmic Ca²⁺ in
703 mouse pancreatic β -cells. *Diabetes* 47: 1266-1273, 1998.
704
- 705 32. **Jonkers FC, Henquin JC**. Measurements of cytoplasmic Ca²⁺ in islet cell
706 clusters show that glucose rapidly recruits β -cells and gradually increases the
707 individual cell response. *Diabetes* 50: 540-550, 2001.
708
- 709 33. **Kalwat MA, Cobb MH**. Mechanisms of the amplifying pathway of insulin
710 secretion in the β cell. *Pharmacol Ther* 179:17-30, 2017.
711

- 712 34. **Karam JH, Sanz N, Salamon E, Nolte MS.** Selective unresponsiveness of
713 pancreatic β -cells to acute sulfonylurea stimulation during sulfonylurea
714 therapy in NIDDM. *Diabetes* 35:1314-1320, 1986.
715
- 716 35. **Lacy PE, Walker MM, Fink CJ.** Perfusion of isolated rat islets in vitro.
717 Participation of the microtubular system in the biphasic release of insulin.
718 *Diabetes* 21: 987-998, 1972.
719
- 720 36. **Landahl HD, Grodsky GM.** Comparison of models of insulin release. *Bull*
721 *Math Biol* 44: 399-409, 1982.
722
- 723 37. **Lenzen S.** Insulin secretion by isolated perfused rat and mouse pancreas. *Am*
724 *J Physiol* 236: E391-E400, 1979.
725
- 726 38. **Lim EL, Hollingsworth KG, Aribisala BS, Chen MJ, Mathers JC, Taylor R.**
727 Reversal of type 2 diabetes: normalisation of beta cell function in association
728 with decreased pancreas and liver triacylglycerol. *Diabetologia* 54: 2506-2514,
729 2011.
730
- 731 39. **Low JT, Mitchell JM, Do OH, Bax J, Rawlings A, Zavortink M, Morgan G,**
732 **Parton RG, Gaisano HY, Thorn P.** Glucose principally regulates insulin
733 secretion in mouse islets by controlling the numbers of granule fusion events per
734 cell. *Diabetologia* 56: 2629-2637, 2013.
735
- 736 40. **Mears D, Sheppard NF Jr, Atwater I, Rojas E, Bertram R, Sherman A.**
737 Evidence that calcium release-activated current mediates the biphasic electrical
738 activity of mouse pancreatic β -cells. *J Membr Biol* 155: 47-59, 1997.
739
- 740 41. **Meissner HP.** Electrical characteristics of the beta-cells in pancreatic islets.
741 *J Physiol (Paris)* 72:757-767, 1976.
742
- 743 42. **Meissner HP, Atwater IJ.** The kinetics of electrical activity of β cells in
744 response to a "square wave" stimulation with glucose or glibenclamide. *Horm*
745 *Metab Res* 8:11-16, 1976.
746
- 747 43. **Mourad NI, Nenquin M, Henquin JC.** Metabolic amplifying pathway
748 increases both phases of insulin secretion independently of β -cell actin
749 microfilaments. *Am J Physiol Cell Physiol* 299: C389-C398, 2010.
750
- 751 44. **Mourad NI, Nenquin M, Henquin JC.** Metabolic amplification of insulin
752 secretion by glucose is independent of β -cell microtubules. *Am J Physiol Cell*
753 *Physiol* 300: C697-C706, 2011.
754
- 755 45. **Nijpels G, Boorsma W, Dekker JM, Hoeksema F, Kostense PJ, Bouter LM,**
756 **Heine RJ.** Absence of an acute insulin response predicts onset of type 2 diabetes
757 in a Caucasian population with impaired glucose tolerance. *J Clin Endocrinol*
758 *Metab* 93:2633-2638, 2008.
759

- 760 46. **Nunemaker CS, Wasserman DH, McGuinness OP, Sweet IR, Teague JC,**
761 **Satin LS.** Insulin secretion in the conscious mouse is biphasic and pulsatile. *Am J*
762 *Physiol Endocrinol Metab* 290: E523-E529, 2006.
763
- 764 47. **O'Connor MD, Landahl H, Grodsky GM.** Comparison of storage- and signal-
765 limited models of pancreatic insulin secretion. *Am J Physiol* 238: R378-R89, 1980.
766
- 767 48. **Olofsson CS, Göpel SO, Barg S, Galvanovskis J, Ma X, Salehi A, Rorsman P,**
768 **Eliasson L.** Fast insulin secretion reflects exocytosis of docked granules in
769 mouse pancreatic B-cells. *Pfluegers Arch* 444: 43-51, 2002.
770
- 771 49. **Pedersen MG, Bertram R, Sherman A.** Intra- and inter-islet synchronization
772 of metabolically driven insulin secretion. *Biophys J* 89: 107-119, 2005.
773
- 774 50. **Pedersen MG, Corradin A, Toffolo GM, Cobelli C.** A subcellular model of
775 glucose-stimulated pancreatic insulin secretion. *Philos Trans A Math Phys Eng Sci*
776 366: 3525-3543, 2008.
777
- 778 51. **Pedersen MG, Sherman A.** Newcomer insulin secretory granules as a highly
779 calcium-sensitive pool. *Proc Natl Acad Sci USA* 106: 7432-7436, 2009.
780
- 781 52. **Pfeifer MA, Halter JB, Porte D Jr.** Insulin secretion in diabetes mellitus. *Am J*
782 *Med* 70: 579-588, 1981.
783
- 784 53. **Porte D Jr.** Banting lecture 1990. Beta-cells in type II diabetes mellitus.
785 *Diabetes* 40: 166-80, 1991.
786
- 787 54. **Pratley RE, Weyer C.** The role of impaired early insulin secretion in the
788 pathogenesis of Type II diabetes mellitus. *Diabetologia* 44:929-945, 2001.
789
- 790 55. **Ravier MA, Güldenagel M, Charollais A, Gjinovci A, Caille D, Söhl G,**
791 **Wollheim CB, Willecke K, Henquin JC, Meda P.** Loss of connexin36 channels
792 alters beta-cell coupling, islet synchronization of glucose-induced Ca²⁺ and
793 insulin oscillations, and basal insulin release. *Diabetes* 54: 1798-1807, 2005.
794
- 795 56. **Ricordi C, Lacy PE, Finke EH, Olack BJ, Scharp DW.** Automated method for
796 isolation of human pancreatic islets. *Diabetes* 37:413-420, 1988.
797
- 798 57. **Rorsman P, Ashcroft FM.** Pancreatic β -cell electrical activity and insulin
799 secretion: of mice and men. *Physiol Rev* 98:117-214, 2018.
800
- 801 58. **Rorsman P, Braun M.** Regulation of insulin secretion in human pancreatic
802 islets. *Annu Rev Physiol* 75:155-179, 2013.
803
- 804 59. **Smolen P, Rinzel J, Sherman A.** Why pancreatic islets burst but single β cells
805 do not. The heterogeneity hypothesis. *Biophys J* 64:1668-1680, 1993.
806
- 807 60. **Speier S, Gjinovci A, Charollais A, Meda P, Rupnik M.** Cx36-mediated
808 coupling reduces β -cell heterogeneity, confines the stimulating glucose

- 809 concentration range, and affects insulin release kinetics. *Diabetes* 56:1078-1086,
810 2007.
- 811
- 812 61. **Stožer A, Dolenšek J, Rupnik MS.** Glucose-stimulated calcium dynamics in
813 islets of Langerhans in acute mouse pancreas tissue slices. *PLoS One* 8: e54638,
814 2013.
- 815
- 816 62. **Stumvoll M, Fritsche A, Häring HU.** Clinical characterization of insulin
817 secretion as the basis for genetic analyses. *Diabetes* 51 Suppl 1:S122-S129, 2002.
- 818
- 819 63. **Toschi E, Camastra S, Sironi AM, Masoni A, Gastaldelli A, Mari A,**
820 **Ferrannini E, Natali A.** Effect of acute hyperglycemia on insulin secretion in
821 humans. *Diabetes* 51 Suppl 1:S130-S133, 2002.
- 822
- 823 64. **Weiss R, Caprio S, Trombetta M, Taksali SE, Tamborlane WV,**
824 **Bonadonna R.** β -cell function across the spectrum of glucose tolerance in obese
825 youth. *Diabetes* 54:1735-1743, 2005.
- 826
- 827 65. **Yasuda T, Shibasaki T, Minami K, Takahashi H, Mizoguchi A, Uriu Y,**
828 **Numata T, Mori Y, Miyazaki J, Miki T, Seino S.** Rim2alpha determines docking
829 and priming states in insulin granule exocytosis. *Cell Metab* 12:117-129, 2010.
- 830
- 831
- 832
- 833

834 **FIGURE LEGENDS**

835

836

837 **Fig. 1: Overview of the three considered models.**

838

839

840 **Fig. 2:**

841 **Experimental data.** Experimental $[Ca^{2+}]_i$ traces (in nM; thick curves, left axes)
 842 and insulin secretion measurements (% of islet content per minute; thin curves
 843 with dots, right axes). Time is in minutes. The data in panels A-G are from
 844 Henquin et al. (ref 29), where glucose (G) was stepped at 0 min (indicated by
 845 arrow) from 3 mM (A-D) or 8.5 mM (E-G) to 8.5, 11.1, 16.7 or 30 mM, as
 846 indicated. The data in panels H-K are from Mourad et al. (ref 43), where islets
 847 were stimulated by either 500 μ M tolbutamide (Tolb) in 3mM glucose or 15 mM
 848 glucose, continuously or in 8 min pulses, as indicated by arrows. The data in
 849 panels L-N are new experiments shown as means for 3 experiments of insulin
 850 secretion and 12-18 islets for $[Ca^{2+}]_i$. In panel L, staircase increase in glucose
 851 from 3 mM to 7 mM, 10 mM and finally 15 mM, in 5 min steps indicated by
 852 arrows, followed by removal of extracellular calcium between 30 and 40 min
 853 (indicated by the bar). In panel M, the steps of the staircase were extended to a
 854 duration of 20 min, as indicated by arrows. In panel N, glucose was stepped from
 855 3 mM to 15 mM at 0 min (arrow), followed by removal of extracellular calcium
 856 between 15 and 25 min (bar).

857

858 **Fig. 3:**

859 **Model 1 results.** Simulated secretion profiles (% of islet content per minute;
 860 axes are shown only once for each row) obtained with Model 1 fitted to the
 861 experimental data (black dots and curves), either with (red curves) or without
 862 (blue curves) the constraint of refilling being a non-decreasing function of the
 863 glucose concentration G . Layout as in Fig. 2. Panel O shows parameters for
 864 refilling ($M(G)$ in % of islet content per minute) with (red) or without (blue) the
 865 monotonicity constraint on $M(G)$.

866

867 **Fig. 4:**

868 **Pool dynamics in Model 1.** Simulated dynamics of RRP (in % of islet content)
 869 obtained with Model 1 for selected protocols as indicated.

870

871 **Fig. 5:**

872 **Model 2 results.** Simulated secretion profiles (% of islet content per minute;
 873 axes are shown only once for each row) obtained with Model 2 fitted to the
 874 experimental data (black dots and curves), either with (red curves) or without
 875 (blue curves) the constraint of refilling and priming being a non-decreasing
 876 function of the glucose concentration G . Layout as in Fig. 2. Panel O shows
 877 parameters for priming ($p(G)$ with unit 1/min; upper, right axis) and
 878 mobilization ($M(G)$ in % of islet content per minute; lower, left axis) with (red)
 879 or without (blue) the monotony constraint on $p(G)$ and $M(G)$.

880

881

882

883 Fig. 6:
884 **Pool dynamics in Model 2.** Simulated dynamics of RRP (thick curves; % of islet
885 content) and X (thin curves; % of islet content) obtained with Model 2 for
886 selected protocols as indicated.

887
888
889 Fig. 7:
890 **Model 3 results.** Simulated secretion profiles (% of islet content per minute;
891 axes are shown only once for each row) obtained with Model 3 fitted to the
892 experimental data (black dots and curves), either with (red curves) or without
893 (blue curves) the constraint of refilling and priming being a non-decreasing
894 function of the glucose concentration G . Layout as in Fig. 2. Panel O shows
895 parameters for priming ($p(G)$ with unit 1/min; upper, right axis) and
896 mobilization ($M(G)$ in % of islet content per minute; lower, left axis) with (red)
897 or without (blue) the monotony constraint on $p(G)$ and $M(G)$.

898
899 Fig. 8:
900 **Pool dynamics in Model 3.** Simulated dynamics of RRP (thick curves; % of islet
901 content) and X (thin curves; % of islet content) obtained with Model 3 for
902 selected protocols as indicated.
903
904

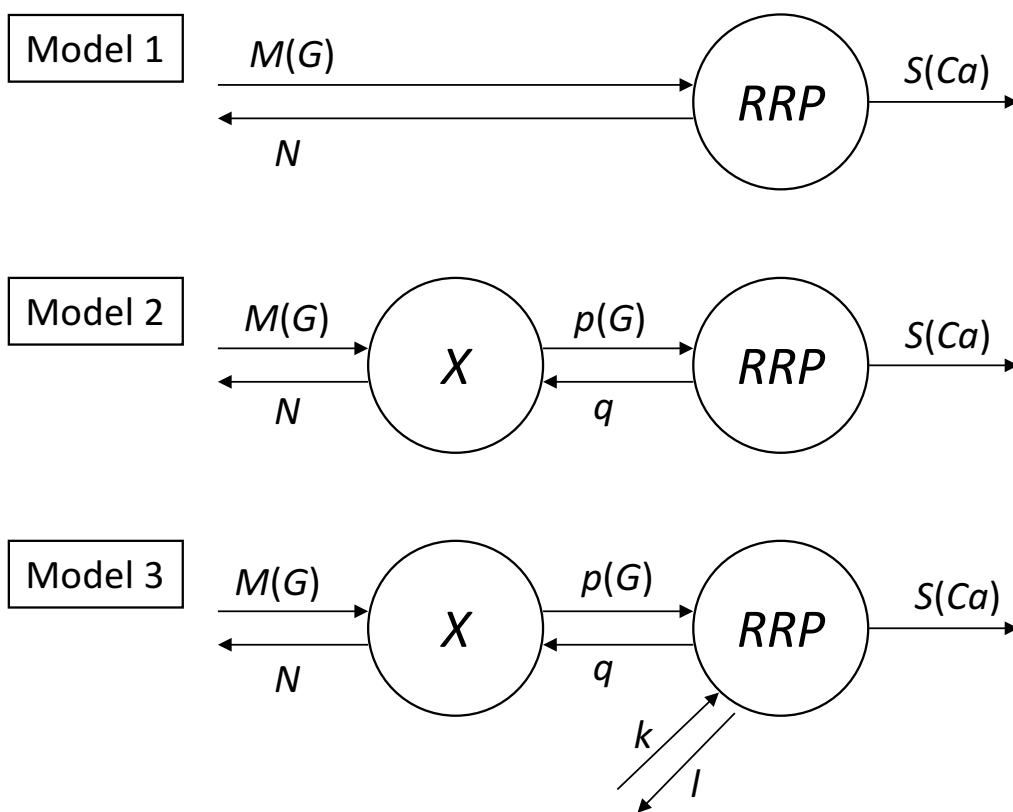


Figure 1

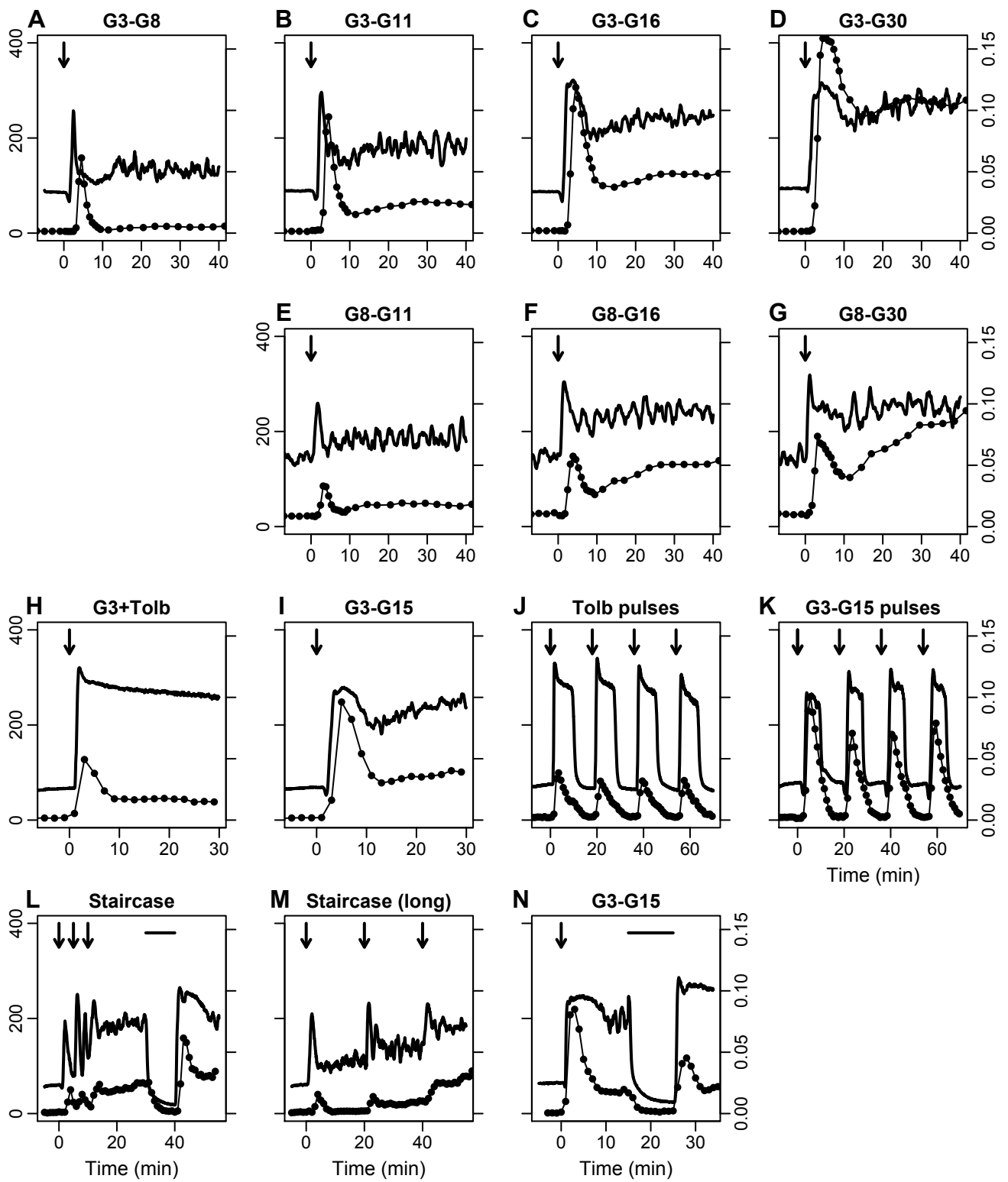


Figure 2

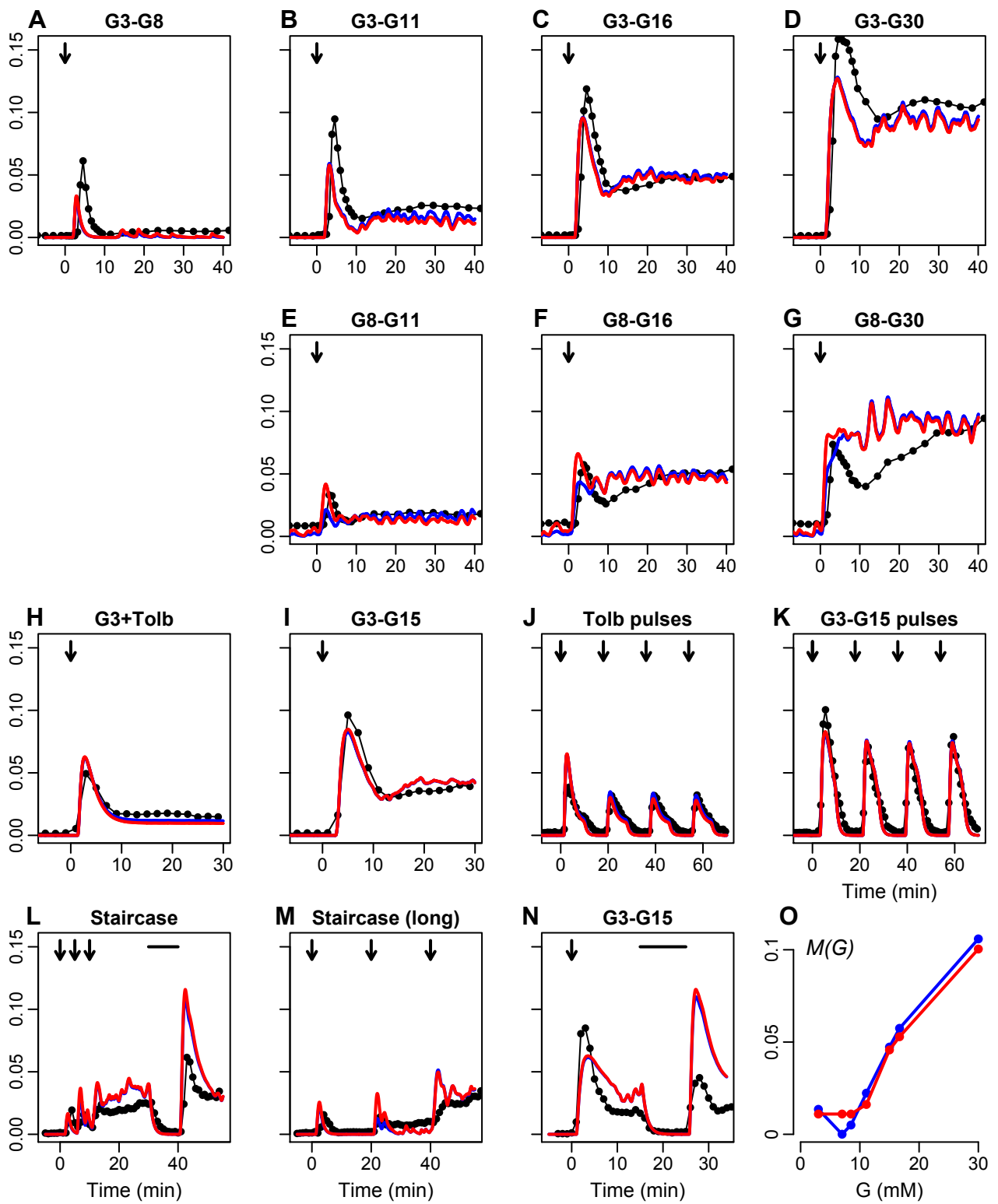


Figure 3

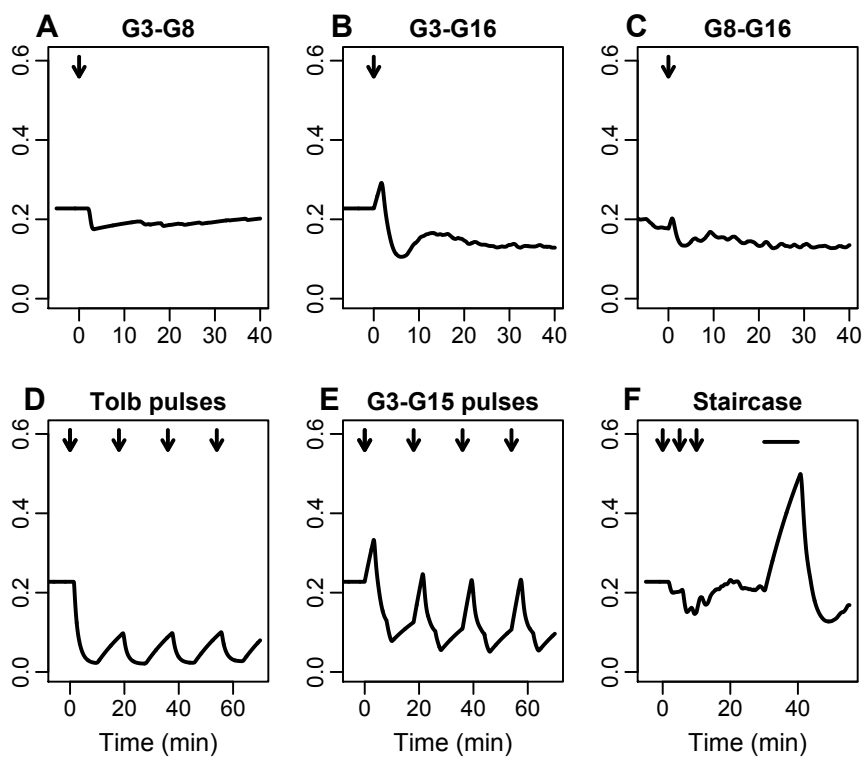


Figure 4

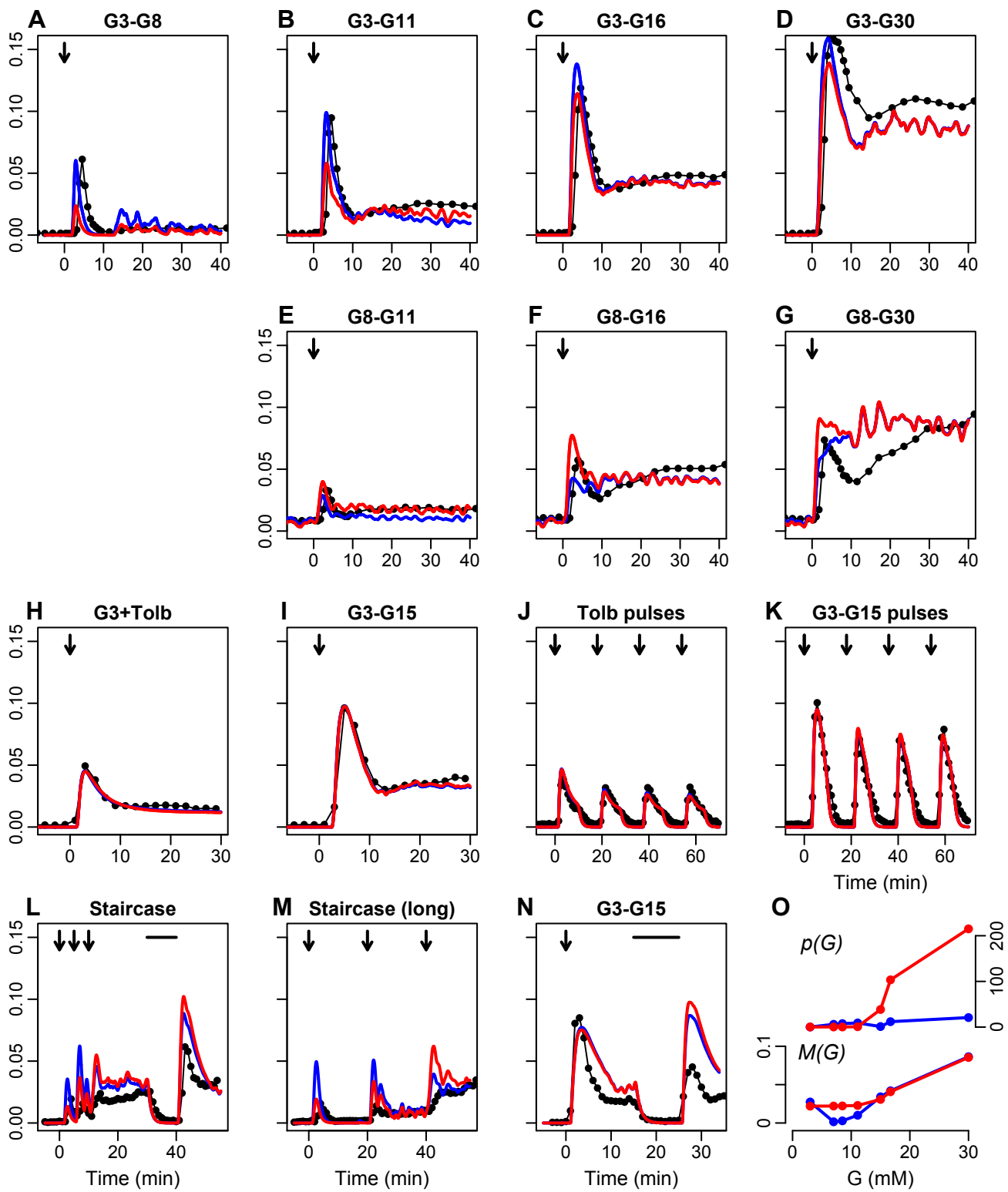


Figure 5

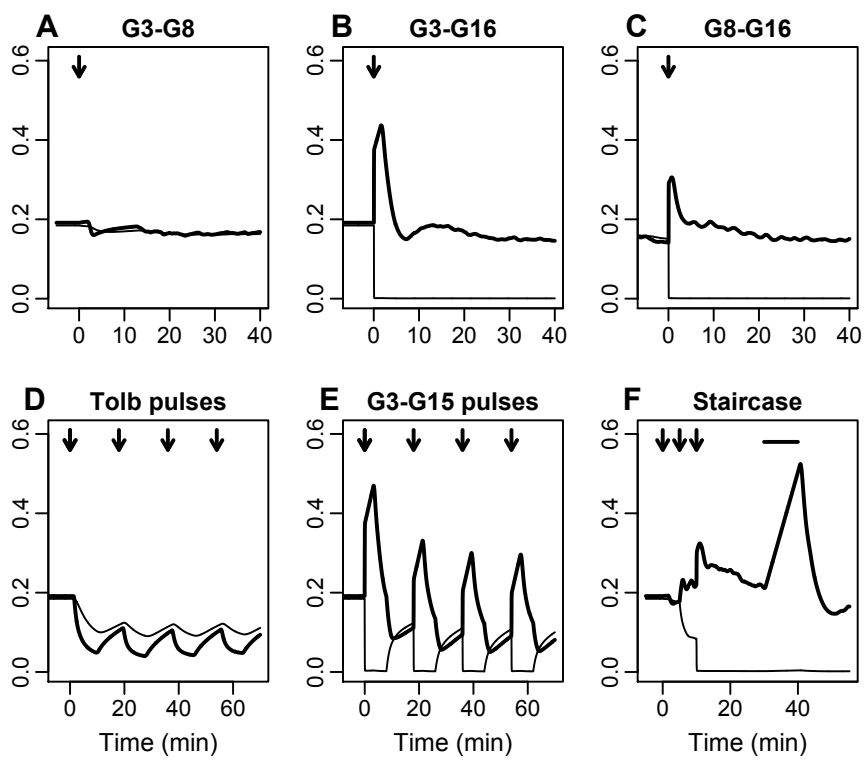


Figure 6

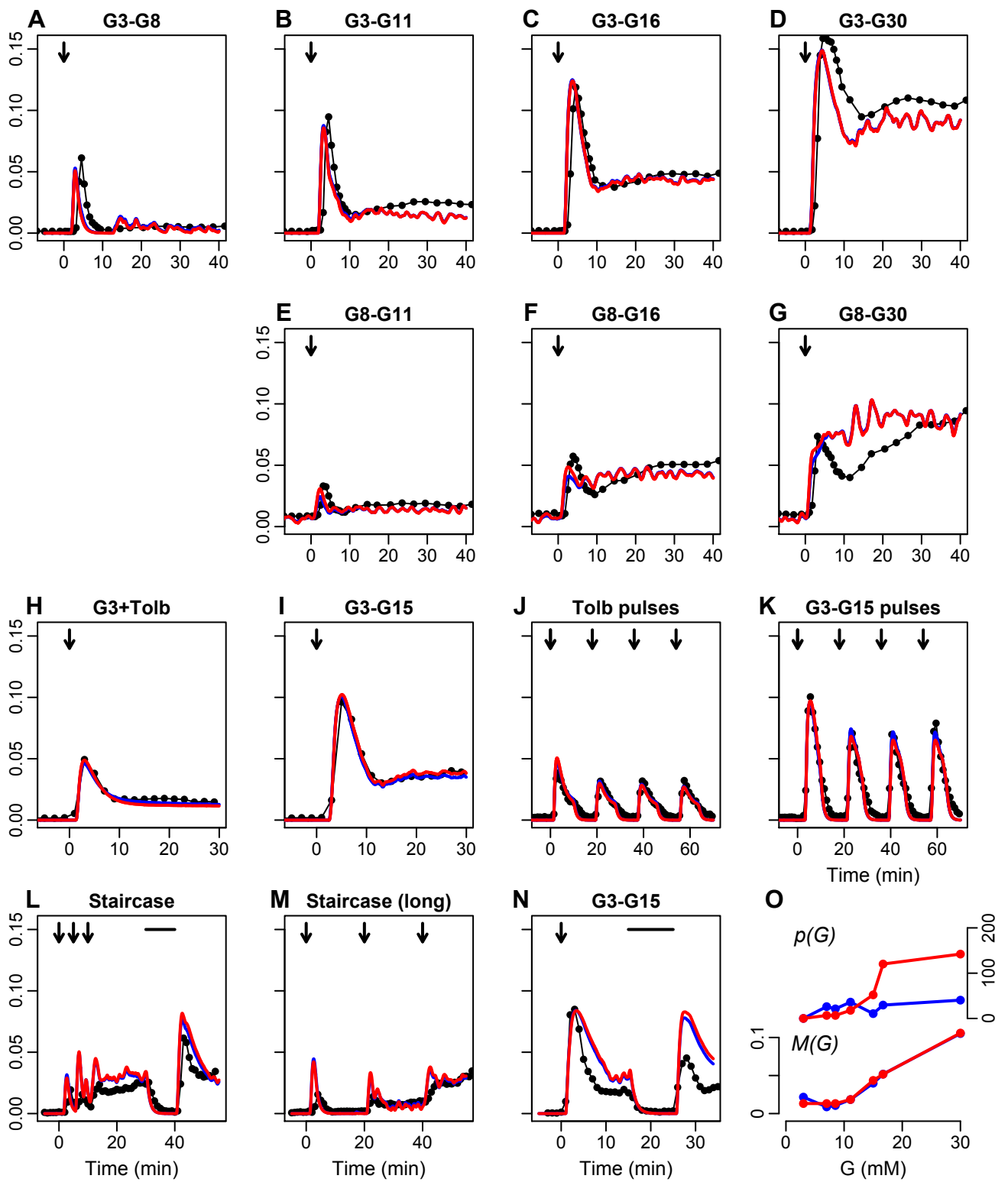


Figure 7

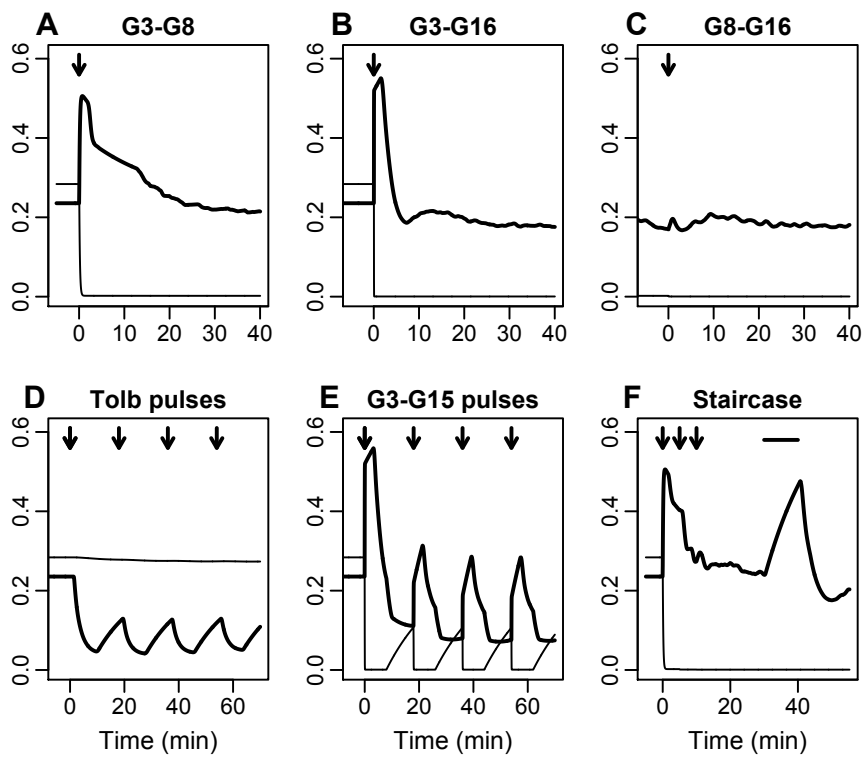


Figure 8